Journal of Sound and Vibration 333 (2014) 2505–2519

Contents lists available at ScienceDirect

Journal of Sound and Vibration

journal homepage: www.elsevier.com/locate/jsvi

Extraction of the acoustic component of a turbulent flow exciting a plate by inverting the vibration problem

D. Lecoq *, C. Pézerat, J.-H. Thomas, W.P. Bi

UNAM Université, Université du Maine, CNRS UMR 6613, Laboratoire d'Acoustique de l'Université du Maine (LAUM), Avenue Olivier Messiaen, 72085 Le Mans Cedex 9, France

ARTICLE INFO

Article history:
Received 22 July 2012
Received in revised form
2 February 2014
Accepted 3 February 2014
Handling Editor: D. Juve
Available online 24 February 2014

ABSTRACT

An improvement of the Force Analysis Technique (FAT), an inverse method of vibration, is proposed to identify the low wavenumbers including the acoustic component of a turbulent flow that excites a plate. This method is a significant progress since the usual techniques of measurements with flush-mounted sensors are not able to separate the acoustic and the aerodynamic energies of the excitation because the aerodynamic component is too high. Moreover, the main cause of vibration or acoustic radiation of the structure might be due to the acoustic part by a phenomenon of spatial coincidence between the acoustic wavelengths and those of the plate. This underlines the need to extract the acoustic part. In this work, numerical experiments are performed to solve both the direct and inverse problems of vibration. The excitation is a turbulent boundary layer and combines the pressure field of the Corcos model and a diffuse acoustic field. These pressures are obtained by a synthesis method based on the Cholesky decomposition of the cross-spectra matrices and are used to excite a plate. Thus, the application of the inverse problem FAT that requires only the vibration data shows that the method is able to identify and to isolate the acoustic part of the excitation. Indeed, the discretization of the inverse operator (motion equation of the plate) acts as a low-pass wavenumber filter. In addition, this method is simple to implement because it can be applied locally (no need to know the boundary conditions), and measurements can be carried out on the opposite side of the plate without affecting the flow. Finally, an improvement of FAT is proposed. It regularizes optimally and automatically the inverse problem by analyzing the mean quadratic pressure of the reconstructed force distribution. This optimized FAT, in the case of the turbulent flow, has the advantage of measuring the acoustic component up to higher frequencies even in the presence of noise.

© 2014 Elsevier Ltd. All rights reserved.

1. Introduction

Turbulences in a flow, caused by boundary layers or the presence of obstacles close to a structure, generate vibrations and can be a major source of noise. In the context of reducing transport noises, this is one of the main acoustic sources with the engine noise. The considerable improvements on this latter and the advent of the new electric vehicles make the aerodynamic noise increasingly become a dominant acoustic source.

* Corresponding author.
E-mail address: damien.lecoq@univ-lemans.fr (D. Lecoq).

http://dx.doi.org/10.1016/j.jsv.2014.02.003
0022-460X © 2014 Elsevier Ltd. All rights reserved.

Vibration problems of a plate excited by a turbulent flow are complex since they are connected to fluid mechanics and vibrations. Studies dealing with these problems are not new, they are numerous and they had often been motivated by boat and aircraft [1,2]. However, they can be adapted to cars where the fluid is light and the speeds are small compared to the speed of sound.

In our study, the source of vibration is a Turbulent Boundary Layer. Existing numerical simulations of this kind of excitation are based on the Navier–Stokes equations such as the Direct Numerical Simulation (DNS). But these methods are very restrictive in terms of computational cost especially if one must take into account the compressibility of the fluid [3]. This is why the semi-empirical models, which need to be experimentally adjusted, are often used. They are classified into two categories, those that model only the aerodynamic part as Corcos [4] or Chase [5] and those that take into account the compressibility of the fluid as the second model of Chase [6] allowing the study of the acoustic component.

Experimentally, the acoustic part is very difficult to assess by usual techniques of measurement, with flush-mounted sensors for example, because the aerodynamic part has a very high amplitude. Even if a sensor array is used to separate the small wavelengths of the aerodynamic component and those of the acoustic that are larger, the latter is embedded in the background noise. This is a major problem, because in many cases, the vibration and the acoustic radiation of the structure can be linked to this component. Recently, Arguillat et al. [7] developed a powerful technique that can measure the two components. However, this technique has two major disadvantages. The first is the difficulty of implementation, because it requires the use of an antenna with 63 sensors embedded in the structure. The second is related to the measurement and the computation time because the pressure must be recorded from 63 angles, the wavenumber–frequency spectra must be calculated for each frequency and interpolated with a theoretical model.

The Force Analysis Technique (FAT) [8] is proposed here to identify this turbulent wall pressure, especially the acoustic part and the low wavenumbers. Thus, the excitation is estimated by measuring the displacement field of the plate and by injecting it into the equation of motion where the spatial derivatives are calculated by a finite difference method. In this way, the acoustic component is measured using the vibration of the plate that is sensitive to excitation in the low wavenumbers. The idea of using the structure as a filter is not new [9]. Martin and Leehey [10] show how it is possible to measure the low wavenumbers with a membrane excited by turbulent wall pressures. This method is a modal approach and requires the knowledge of the boundary conditions, which is a limitation for industrial applications. The FAT method, that we propose to use in this paper, is local and there is no need to know the boundary conditions to compute it.

This paper was motivated by the results of a first experimental study [11]. The authors wanted to use FAT in order to measure the wall pressure fluctuations beneath a turbulent boundary layer in a wind tunnel. Finally, they identified a spectrum 20 dB below the spectrum measured by a flush-mounted sensor and this is about the same gap found by Arguillat et al. [6] between the aerodynamic and the acoustic components in the same wind tunnel. Chevillotte et al. therefore hypothesized that the method identifies the acoustic component of the TBL. This is confirmed by the presence of resonance peaks in the spectrum corresponding to the frequencies of transverse acoustic modes of the tunnel. The simulations proposed in this paper allow us to confirm this hypothesis since the excitation signals are well known. Through these simulations, where we can control the excitation and the SNR, we have developed an optimization method for the regularization of FAT in the case of the identification of the low wavenumbers in turbulent wall pressures.

In order to test this method, a numerical simulation (Fig. 1) is implemented, the parameters of which are close to the experimental conditions. That is why, time signals are used and some noise is added to the displacement fields. First, the characteristics of the studied aeroacoustic sources are presented. The direct problem of Fig. 1 is then described in Section 3. The pressure signals, resulting from a synthesis method based on the Cholesky decomposition, correspond to the Corcos model and to a diffuse acoustic field. The displacement field is calculated by modal decomposition. Then the forces identified by FAT in the inverse problem are compared with the excitation signals in Section 4. The first simulations concern only the diffuse field in order to set the inverse method and the regularization of FAT is improved by analyzing the mean quadratic pressure of the reconstructed fields. Unlike the classical method FAT where the regularization is set by the user and constant with frequency, this enhancement allows FAT to automatically and objectively regularize the inverse problem at each frequency. Finally, FAT and its optimization are tested on the synthesized turbulent pressures.

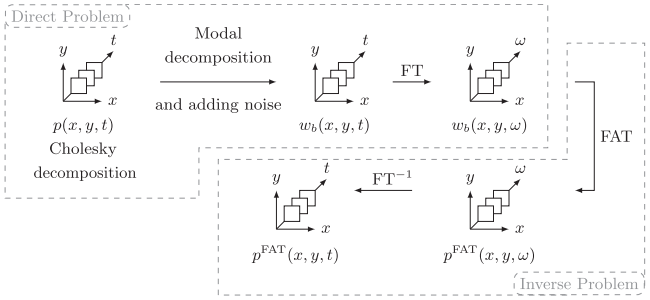

Fig. 1. Synopsis of simulations: the excitation, the direct and inverse problems of vibration where p denotes the pressure field that excites the structure, w the displacement of the plate and FT the Fourier Transform.

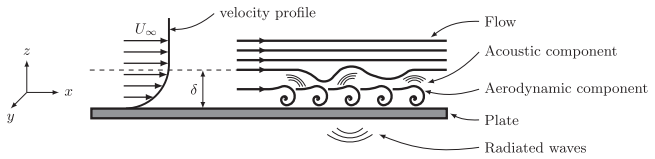

Fig. 2. Vibrating plate excited by a TBL where U_∞ is the fluid velocity and δ is the boundary layer thickness.

2. Overview of aeroacoustic source characteristics

This section presents the characteristics of the studied excitation $p(x,y,t)$ which is a Turbulent Boundary Layer (TBL). The resulting wall pressure is decomposed into two parts as shown in Fig. 2:

- the aerodynamic component characterized by the convection wavenumber [12]

$$k_{\text{conv}} = \frac{\omega}{U_c}, \tag{1}$$

  where U_c is the convection velocity, generally deduced from the relationship $U_c = KU_\infty$ with U_∞ the fluid velocity in the laminar flow and K a coefficient between 0.6 and 0.8 [12,13];
- the acoustic component related to waves generated by turbulence at the top of the plate and propagating in all directions with the acoustic wavenumber

$$k_{\text{ac}} = \frac{\omega}{c_0}, \tag{2}$$

  where c_0 refers to the speed of sound. Note that this component may also contain contributions due to the plate vibration. This is particularly true if the problem is in the vicinity of the coincidence frequency and when the coupling effects between the plate and the fluid are not negligible. In this study, there is therefore no separation between the acoustic radiation of the plate and the acoustic part of the TBL.

Generally, the wavenumber–frequency spectra $S_{pp'}(k_x,k_y,\omega)$ are used to analyze these excitations [12]

$$S_{pp'}(k_x,k_y,\omega) = \frac{1}{4\pi^2}\iint_{-\infty}^{+\infty} S_{pp'}(r_x,r_y,\omega)\mathrm{e}^{-jk_x r_x}\mathrm{e}^{-jk_y r_y}\,\mathrm{d}r_x\,\mathrm{d}r_y, \tag{3}$$

where $r_x = x - x'$, $r_y = y - y'$, and $S_{pp'}(r_x,r_y,\omega)$ the cross-spectrum between the wall pressures $p(x,y,t)$ and $p(x',y',t)$

$$S_{pp'}(r_x,r_y,\omega) = \lim_{T\to\infty}\frac{2\pi}{T}\mathrm{E}\left[P(x,y,\omega)P^*(x',y',\omega)\right], \tag{4}$$

where $P(x,y,\omega)$ is the finite Fourier transform of $p(x,y,t)$ with T the duration of the signal

$$P(x,y,\omega) = \frac{1}{2\pi}\int_{-T/2}^{T/2} p(x,y,t)\mathrm{e}^{j\omega t}\,\mathrm{d}t, \tag{5}$$

and $P^*(x,y,\omega)$ its complex conjugate.

With this kind of representation, one can easily distinguish the two components: the acoustic component in the low wavenumbers and the aerodynamic component with very small wavelengths (see Fig. 3). In addition, the wavenumber representation allows one to study the vibration and the radiation of a plate under TBL conditions by introducing the flexural wavenumber k_f [14]:

$$k_f = \sqrt[4]{\frac{12\rho(1-\nu^2)}{Eh^2}}\sqrt{\omega}, \tag{6}$$

where ρ, E, ν are respectively the mass density, Young's modulus, Poisson's ratio of the material and h is the thickness of the plate.

Fig. 3 shows the evolution of this wavenumber as a function of frequency in parallel with that of the aerodynamic and the acoustic components. In this study, the convection velocity is much lower than the speed of sound (low Mach number). Therefore, the slope of the k_{conv} line is higher than the slope of the k_{ac} line (Eqs. (1) and (2)), and the aerodynamic coincidence obtained at the angular frequency ω_{conv} for $k_{conv} = k_f$ is in the very low frequencies whereas the acoustic coincidence obtained at ω_{ac} for $k_{ac} = k_f$ is in the very high frequencies. In the wavenumber domain, the aerodynamic energy is located around the point $k_x = k_{\text{conv}}$ (where x is the direction of the flow) and most of this energy moves rapidly toward the high wavenumbers when increasing the frequency. The acoustic part is mainly located around the origin in a circle with a radius equal to k_{ac} and according to Eq. (2), this radius grows with the frequency.

One important characteristic of the excitation is that the aerodynamic component has an amplitude much higher than the acoustic one [18]. However, the convection wavenumber is very high whereas the acoustic and flexural wavenumbers

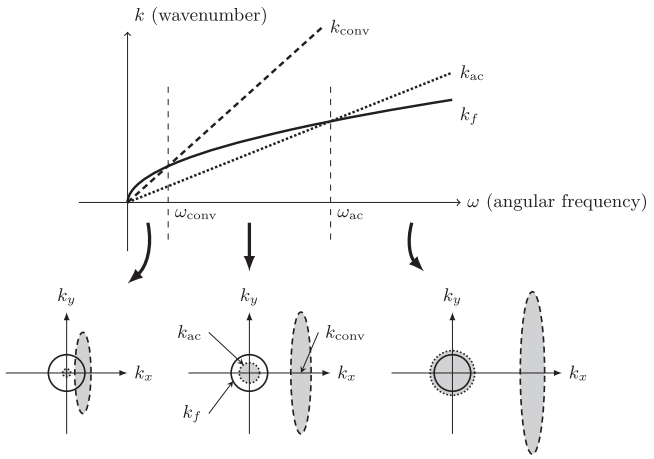

Fig. 3. Flexural (—— solid line), convection (- - - dashed line) and acoustic (··· dotted line) wavenumbers with respect to the angular frequency ω. The wavenumber–frequency spectrum of the excitation is shown schematically for three frequency ranges [12]: before the aerodynamic coincidence $\omega < \omega_{conv}$, in the mid-frequency region $\omega_{conv} < \omega < \omega_{ac}$ and after the acoustic coincidence $\omega > \omega_{ac}$.

have the same order of magnitude in a wide frequency range (see Fig. 3). That is the reason why the vibration and the radiation of the plate are very sensitive to the acoustic part.

3. Direct problem: numerical experiment

The purpose of this section is to present a simulated experiment that is implemented in order to test the identification of turbulent wall pressures by FAT. The direct problem of vibration presented in Fig. 1 simulates experimental conditions with additive noise in the vibration signals given in the time domain. The main goal of this simulation test is to see how solving the inverse problem yields identifying the efforts of which the wavenumber–frequency and the frequency spectra are representative of a TBL.

This section presents the full resolution of the direct problem of a plate excited by a TBL: the excitation signals (models and synthesis) and the direct problem of vibration.

3.1. Aerodynamic component: Corcos model

In this study, the origin of the turbulent flow is related to turbulent boundary layers. There are some frequency spectrum models and they are wisely reviewed by Hwang et al. [15]. It is shown that the semi-empirical model of Goody [16] seems to fit the experimental results in the best way. It is true for a very wide range of flow velocities because the model takes into account the Reynolds number through a parameter called R_T. Therefore, this model is used in the simulations and its expression is given by

$$S_{pp}(\omega) = \frac{3\tau_w^2 \delta \left(\frac{\omega\delta}{U_\infty}\right)^2}{U_\infty \left(\left[0.5 + \left(\frac{\omega\delta}{U_\infty}\right)^{0.75}\right]^{3.7} + \left[1.1\ R_T^{-0.57}\left(\frac{\omega\delta}{U_\infty}\right)\right]^7 \right)}, \tag{7}$$

with $R_T = u_*^2 \delta/\nu U_\infty$, and where u_*, δ, ν', τ_w are respectively the friction velocity, the boundary layer thickness, the kinematic coefficient of viscosity and the wall shear stress. The numerical values of these parameters are given by Farabee and Casarella [17] and by Hwang et al. [15].

There are also some models of wavenumber–frequency spectra. Howe [18] offers a detailed description of the main models. For the aerodynamic part, the Corcos model [4] for which it is assumed that the fluid is incompressible is often used because it is very easy to implement. It does not consider the acoustic part. This model defines the cross-spectrum between two points by combining a term of propagation along x, and two decreasing exponentials describing the correlation lengths along x and along y:

$$S_{pp'}^{aero}(r_x, r_y, \omega) = S_{pp}(\omega)\, \mathrm{e}^{-\omega(|r_x|/\alpha_x U_c)} \mathrm{e}^{-\omega(|r_y|/\alpha_y U_c)} \mathrm{e}^{j\omega(r_x/U_c)}, \tag{8}$$

where the coefficients α_x and α_y define the decay of the spatial coherence.

3.2. Acoustic component: diffuse field

The aim of the study is to understand how the inverse method FAT identifies the excitations with a cross-spectrum similar to that of the turbulent wall pressures. That is why there is no attempt to accurately model the force field from a TBL.

Thus, the acoustic component is artificially added to the Corcos model using a diffuse field [19]:

$$S^{\mathrm{ac}}_{pp'}(r_x, r_y, \omega) = AS_{pp}(\omega)\mathrm{sinc}\left(k_{\mathrm{ac}}\sqrt{r_x^2+r_y^2}\right). \tag{9}$$

The coefficient A reflects the relationship between the aerodynamic and the acoustic energies. In this way, the total cross-spectrum of the wall pressure can be modelled from Eqs. (8) and (9):

$$S_{pp'}(r_x, r_y, \omega) = S_{pp}(\omega)\left(\mathrm{e}^{-\omega(|r_x|/\alpha_x U_c)}\mathrm{e}^{-\omega(|r_y|/\alpha_y U_c)}\mathrm{e}^{j\omega(r_x/U_c)} + A\ \mathrm{sinc}\left(k_{\mathrm{ac}}\sqrt{r_x^2+r_y^2}\right)\right). \tag{10}$$

Once again, there is no attempt to model exactly the excitation. The aim is only to see how the inverse problem allows one to identify this kind of excitation for which the acoustic level is much lower than the aerodynamic one. The choice of the coefficient A can be questionable, but in this study its value is set to 5 percent and corresponds to a ratio measured by Arguillat et al. [7] on a particular case of TBL in a wind tunnel. Additional simulations were computed with coefficients lower than 5 percent and the conclusions presented later in Section 4.2.2 remain the same.

3.3. Synthesis of time signals complying with a cross-spectrum template: Corcos model and diffuse field

This section describes how to synthesize the time signals $p(x, y, t)$ which correspond to the sum of the Corcos model and a diffuse acoustic field. A technique presented by Wittig and Sihna [20] provides the simulation of multicorrelated random processes. Recently, Hekmati et al. used this method for turbulent wall pressures [21]. A simplified explanation of this method is proposed here:

1. write the cross-spectrum matrix $\mathbf{S}(\omega)$ in which each term is the Corcos and diffuse field cross-spectrum $S_{pp'}(r_x, r_y, \omega)$ between two points calculated from Eq. (10). With M points in the space domain, $\mathbf{S}(\omega)$ is a $(M \times M)$ matrix;
2. factorize the matrix $\mathbf{S}(\omega)$ by the Cholesky decomposition

$$\mathbf{S}(\omega) = \mathbf{H}(\omega)\mathbf{H}^H(\omega), \tag{11}$$

   where $\mathbf{H}(\omega)$ is a lower triangular matrix and $\mathbf{H}^H(\omega)$ its conjugate transpose;
3. generate a vector $\boldsymbol{\Gamma}$ of random phases with M elements

$$\boldsymbol{\Gamma}_i = \mathrm{e}^{j2\pi\gamma_i}, \tag{12}$$

   where γ_i is a uniformly distributed random number between 0 and 1. We note that the expected value of each element is

$$\mathrm{E}[\Gamma_i] = 0; \tag{13}$$

4. create a vector $\mathbf{P}(\omega)$ for a given angular frequency ω

$$\mathbf{P}(\omega) = \mathbf{H}(\omega)\boldsymbol{\Gamma}. \tag{14}$$

   Each element of the vector $\mathbf{P}(\omega)$ represents the Fourier transform at the angular frequency ω of the time signals $p(x, y, t)$.
5. In the end, steps 1 through 4 are performed for each angular frequency ω up to the Nyquist frequency $f_e/2$. An inverse Fourier transform provides the time signals $p(x, y, t)$.

We can prove easily that the cross-spectrum matrix $\mathbf{S_P}(\omega)$ of the field $\mathbf{P}(\omega)$ in Eq. (14) corresponds to that desired $\mathbf{S}(\omega)$, the cross-spectrum matrix of the Corcos model and a diffuse acoustic field. Indeed, $\mathbf{S_P}(\omega)$ which is obtained using Eq. (4) yields

$$\mathbf{S_P}(\omega) = \mathrm{E}[\mathbf{P}(\omega)\mathbf{P}^H(\omega)]. \tag{15}$$

By replacing $\mathbf{P}(\omega)$ by its expression (14), it becomes

$$\mathbf{S_P}(\omega) = \mathrm{E}[\mathbf{H}\boldsymbol{\Gamma}[\mathbf{H}\boldsymbol{\Gamma}]^H] = \mathrm{E}[\mathbf{H}\boldsymbol{\Gamma}\boldsymbol{\Gamma}^H\mathbf{H}^H] = \mathbf{H}\ \mathrm{E}[\boldsymbol{\Gamma}\boldsymbol{\Gamma}^H]\mathbf{H}^H. \tag{16}$$

According to Eq. (13) and since the random numbers γ_i are independent, the expected value $\mathrm{E}[\boldsymbol{\Gamma}\boldsymbol{\Gamma}^H]$ is the identity matrix $\mathbf{I}$. Finally, according to Eq. (11)

$$\mathbf{S_P}(\omega) = \mathbf{S}(\omega). \tag{17}$$

The pressure field $\mathbf{P}(\omega)$ complies with the Corcos and diffuse field cross-spectrum.

3.4. Results of the synthesis

Results are shown in Fig. 4 where the estimated wavenumber–frequency spectra are calculated by averaged periodograms with segments of 128 points and 50 percent overlap between adjacent blocks that are weighted by a Hann window which allows 14 averages. The numerical values of the TBL parameters are gathered in Table 1 and those of the synthesis in Table 2. The parameters of the TBL are given by Hwang [15]. Coefficients α_x and α_x are found in the literature for smooth walls [12,13,22].

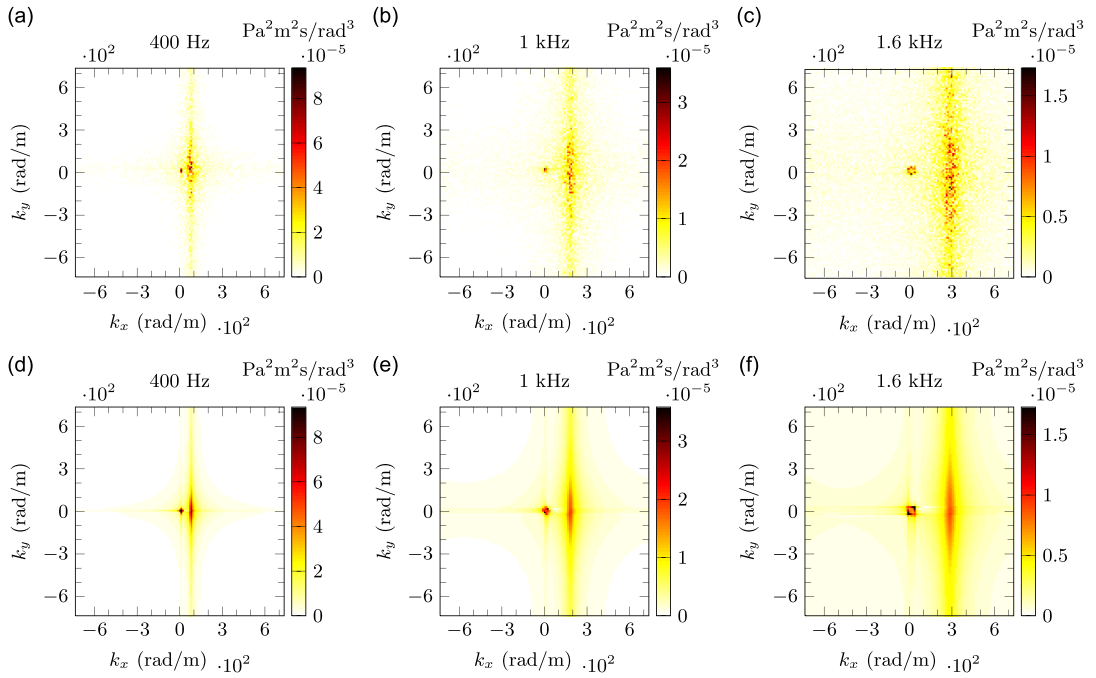

Fig. 4. Wavenumber–frequency spectra $S_{pp'}(k_x, k_y, \omega)$ of the synthesized time signals which correspond to the sum of the Corcos model and a diffuse acoustic field for three different frequencies: (a) 400 Hz, (b) 1 kHz and (c) 1.6 kHz. The theoretical wavenumber–frequency spectra are shown for the same frequencies in (d)–(f).

Table 1
Numerical values of the TBL parameters.

Fluid velocity	$U_\infty = 50$ m/s	Kinematic viscosity	$\nu' = 1.54 \times 10^{-5}$ m²/s
Convection velocity	$U_c = 35$ m/s	Wall shear stress	$\tau_w = 3$ N/m²
Friction velocity	$u_* = 1.58$ m/s	Corcos coefficients	$\alpha_x = 8$; $\alpha_y = 1$
Boundary layer thickness	$\delta = 11.4$ cm		

The wavenumber–frequency spectra of Fig. 4 correspond to the model according to Eq. (10). The aerodynamic part characterized by the convective peak moves towards the high wavenumbers when the frequency increases, while the acoustic component, a circle centered at (k_x=0, k_y=0), excites more wavenumbers in the high frequencies.

Fig. 5 shows the spectrum of the synthesized time signals computed by an averaged periodogram with the same parameters as mentioned previously and averaged over the entire spatial domain. It matches again with the chosen model of frequency spectrum. These signals are used to test FAT and will be used as excitations for the direct problem discussed in the next section.

3.5. Calculation of the vibration

Modal decomposition, method explained by Guyader [14], is used for the calculation of the vibration. This method allows us to have a displacement field $w(x, y, t)$ in the negative z direction (in order to be close to the experimental conditions). Let us consider a rectangular plate whose dimensions are L_x and L_y along x and y (these lengths correspond to those in Table 2) and excited by a pressure field $p(x, y, t)$, the equation of motion and the boundary conditions are

$$\begin{cases} \rho h \dfrac{\partial^2 w}{\partial t^2} + D\left(\dfrac{\partial^4 w}{\partial x^4} + \dfrac{\partial^4 w}{\partial y^4} + 2\dfrac{\partial^4 w}{\partial x^2 \partial y^2}\right) = p(x, y, t), & \text{(a)} \\ w(x, y, t) = \dfrac{\partial^2 w}{\partial x^2} = 0 \text{ for } x = 0 \text{ and } x = L_x, & \text{(b)} \\ w(x, y, t) = \dfrac{\partial^2 w}{\partial y^2} = 0 \text{ for } y = 0 \text{ and } y = L_y, & \text{(c)} \end{cases} \tag{18}$$

Table 2
Spatial and temporal parameters of the synthesis.

Dimensions	$L_x = L_y = 0.5$ m	Sampling frequency	$f_e = 4$ kHz
Discretization	$\Delta_x = \Delta_y = 0.4$ cm	Number of samples	$N = 1000$

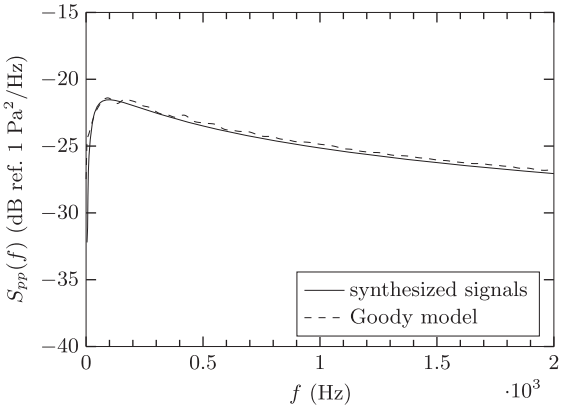

Fig. 5. Comparison between the Goody model and the Power Spectral Density (PSD) of time signals synthesized by the Cholesky decomposition.

with $D = Eh^3/12(1-\nu^2)$. The displacement is decomposed on the normalized eigenfunctions $\phi_{m,n}(x,y)$

$$w(x,y,t) = \sum_{m=1}^{\infty}\sum_{n=1}^{\infty} a_{mn}(t)\ \phi_{mn}(x,y), \tag{19}$$

where $\phi_{mn}(x,y) = (2/\sqrt{L_xL_y})\sin(m\pi x/L_x)\sin(n\pi y/L_y)$. After projection of Eq. (18a) on eigenfunctions $\phi_{mn}(x,y)$ and the heuristic introduction of a modal damping term [14], the coefficients $a_{mn}(t)$ of Eq. (19) verify

$$\ddot{a}_{mn}(t) + 2\zeta_{mn}\omega_{mn}\ \dot{a}_{mn}(t) + \omega_{mn}^2 a_{mn}(t) = \frac{p_{mn}(t)}{\rho h}, \tag{20}$$

where $p_{mn}(t)$ refers to the projection of $p(x,y,t)$ on eigenfunctions $\phi_{mn}(x,y)$, $\omega_{mn} = \sqrt{K_{mn}/\rho h}$ is the natural angular frequency with $K_{mn} = D((m\pi/Lx)^4 + (n\pi/Ly)^4 + 2(m\pi/Lx)^2(n\pi/Ly)^2)$, $\zeta_{mn} = \lambda_{mn}/2\rho h\omega_{mn}$ is the damping ratio and λ_{mn} the generalized damping. Without loss of generality the damping is artificially constant with the order of the eigenmode in order to simplify the problem. The impulse response of the system defined by Eq. (20) is

$$h_{mn}(t) = \frac{e^{-\zeta\omega_{mn}t}}{\sqrt{1-\zeta^2}\omega_{mn}}\ \sin\left(\sqrt{1-\zeta^2}\omega_{mn}t\right). \tag{21}$$

Finally, coefficients $a_{mn}(t)$ are obtained by a convolution such as

$$a_{mn}(t) = \int_{-\infty}^{+\infty} h_{mn}(t-\tau)\frac{p_{mn}(\tau)}{\rho h}\ \mathrm{d}\tau, \tag{22}$$

and provides the displacement of Eq. (19).

The inverse problem tested here to identify the turbulent wall pressure is an experimental technique that requires a regularization in the presence of noise. To simulate experimental conditions, some noise is added to the displacement

$$w_b(x,y,t) = w(x,y,t) + b(x,y,t), \tag{23}$$

where $b(t)$ is a normally distributed random signal with zero mean and a standard deviation σ. The latter is adjusted in order to have a given Signal to Noise Ratio (SNR), defined as the ratio at each point between the power of the signal $w(x,y,t)$ and that of the noise $b(x,y,t)$.

3.6. The studied plate

The structure excited by this TBL is a glass plate with a thickness equal to 3.85 mm. This is the typical case of a windscreen and its parameters are given in Table 3. The number of modes N_{mn} in the plate model depends on the maximum of the wavenumber spectrum for the last mode (m,n) which has the highest order. This maximum should be in higher wavenumbers than the aerodynamic part.

The theoretical evolution of the aerodynamic and acoustic wavenumbers as a function of frequency is shown together and with the flexural wavenumber of the glass plate in Fig. 6. The parameters used in the Corcos model are given in Table 1.

Table 3
Plate parameters.

Young's modulus	$E = 70 \times 10^9$ Pa	Poisson's ratio	$\nu = 0.22$
Density	$\rho = 2700$ kg/m^3	Damping	$\zeta = 0.05$
Thickness	$h = 3.85$ mm	Number of modes	$N_{mn} = 125 \times 125$

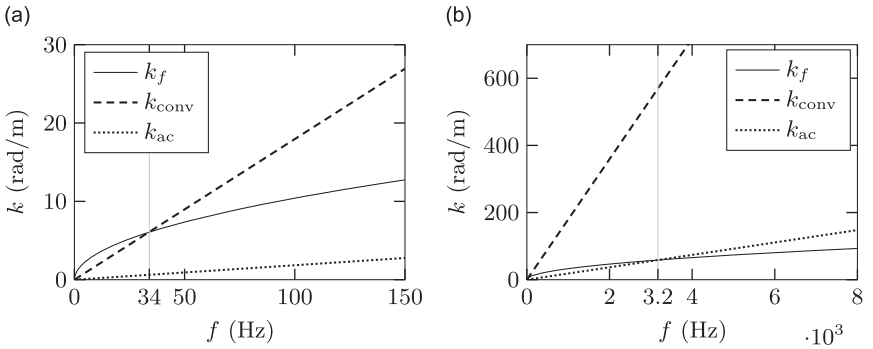

Fig. 6. Flexural, convection and acoustic wavenumbers with respect to the frequency for the studied case. Aerodynamic and acoustic coincidences (vertical lines) are shown in (a) the low frequencies (from 0 to 150 Hz); (b) the high frequencies (from 0 to 8 kHz).

The aerodynamic coincidence is at very low frequencies ($f_{\text{conv}} = 34$ Hz) because the slope of k_{conv} is very high, while the acoustic coincidence is at frequency $f_{\text{ac}} = 3.2$ kHz. According to Fig. 3, in this case, the aerodynamic component moves very quickly towards the high wavenumbers as the frequency increases and the acoustic part has the strongest influence on the vibration and radiation of the wall since the acoustic and flexural wavenumbers are of the same order of magnitude over a wide frequency range.

4. Inverse problem: identification of the wall pressure

4.1. The Force Analysis Technique (FAT)

Let us consider the plate described by Eq. (18a). In FAT, the force distribution is estimated by injecting the displacement field in this equation. For this, the spatial derivatives are calculated by finite difference schemes. The discretized equation of motion to calculate the force distribution at point (i,j) is

$$p_{i,j}^{\text{FAT}} = D(\delta_{i,j}^{4x} + \delta_{i,j}^{4y} + 2\delta_{i,j}^{2x2y}) - \rho h \omega^2 w_{i,j}, \tag{24}$$

where $\delta_{i,j}^{4x}$, $\delta_{i,j}^{4y}$ and $\delta_{i,j}^{2x2y}$ are given in [23]. It requires 13 points of measured displacement around the point (i,j) to compute them. The previous studies show that it is possible to reduce the discretization up to 2 points per flexural wavelength [24].

The major problem with this kind of method is the amplification of measurement errors. Indeed, the estimation of the fourth derivative in the plate equation is very sensitive to short wavelengths related to the measurement noise. A regularization of FAT is proposed to avoid this. It consists in applying a spatial windowing and a low-pass wavenumber filtering on the reconstructed force. In practice, the cutoff wavenumber k_c^{FAT} is defined by

$$k_c^{\text{FAT}} = a \cdot k_f, \tag{25}$$

where a is generally equal to 1, 2, 3 or 4 depending on the Signal to Noise Ratio (SNR) [23].

In this study, the spatial window is a Tukey function which weights the force at the boundaries of the domain over a length equal to $\lambda_c^{\text{FAT}} = 2\pi/k_c^{\text{FAT}}$ [23]. The filtering was performed by a spatial convolution between the force and a sinc function windowed by a Hanning function of length $2\lambda_c^{\text{FAT}}$ [23].

Although the choice of the regularization coefficient a depends on the subjective evaluation of noise, this method gives very good results [25]. However, an improvement of this regularization is proposed in this paper in order to automatically and objectively calculate the optimal coefficient a at each frequency. Thus, it widens the frequency range for which the method is valid. This optimization is described in the following.

Note that the problem to calculate the force distribution from the displacement (and not the inverse) gives an interesting and a non-usual point of view. Indeed, this inverse problem can be seen as a linear shift-invariant system in the space domain while the usual direct problem (the calculation of the displacement from the force distribution) is not, due to the boundaries of the structure. This is due to the fact that only the equation of motion is considered here; the boundary conditions appear in the calculated force distribution as forces and moments located at the edges. In terms of wavenumber analysis, the fact that the studied problem is a linear shift-invariant system implies that there is no wavenumber conversion

between the vibration and the excitation in the inverse problem. The wavenumber components of the vibration field due to other wavenumber components in the excitation give zero when it is injected in the equation of motion, except at the boundaries.

The pressure exciting the plate can then be identified in the whole surface of the plate. Of course, the finite dimensions of the plate restrict the calculation of the wavenumber spectrum of the excitation, because the parietal pressure cannot be identified outside the plate boundaries. Computed wavenumber spectra correspond nevertheless to those of the truncated wall pressure exciting the plate in the studied area.

4.2. Results

4.2.1. Preliminary study: identification of the diffuse field

A preliminary study is proposed to set the inverse method FAT. In this part, only the diffuse field is used in the direct problem. Thus, the cross-spectrum of the excitation is only that of Eq. (9). This first setup allows us to study the high frequencies without having a strong spatial discretization which considerably reduces the computation time. Table 4 shows the simulation parameters, whereas the parameters of the excitation and the plate are shown in Tables 1 and 3. In this study, mesh grids of the force distribution and the displacement field are the same. M is then the number of points in the entire space domain.

The result presented in Fig. 7 is the identification of the diffuse field by the inverse operator, without noise on the displacement and without any regularization. Thereafter this solution is considered as the reference and the optimal solution of FAT. Acoustic coincidence f_{ac} is represented by a dashed line. From about 200 Hz, the lower limit associated with the size of the measurement region, and up to this frequency (3.2 kHz according to Fig. 6), the method is able to reconstruct the whole acoustic energy. But after this coincidence, the acoustic energy is not entirely reconstructed. FAT cancels the filtering of the excitation due to the vibration of the plate and the excitation could be fully identified for these frequencies (higher than 3.2 kHz). However, using the finite difference scheme to estimate the spatial derivatives in the inverse problem of Eq. (24) implies a discretization with a spacing between sensors that causes a low-pass filtering in the wavenumber domain of the solution. This phenomenon is studied by Leclère and Pézerat in [24], where the authors show that the cutoff of this filter is close to the flexural wavenumber k_f. It explains why FAT does not identify the diffuse field after the acoustic coincidence because the excitation in the wavenumber domain is not entirely located inside the circle of radius k_f. The chosen discretization, that sets the transfer function of this filter [24], in this particular case allows the method to capture the acoustic component up to about 4.5 kHz (to an accuracy of 1 dB).

Noise then is added to the displacement field with a SNR equal to 40 dB. The force distributions identified by FAT for different values of the regularization parameter a are compared in Fig. 8. The first observation is the high variability of the spectra obtained with the different values of a. While the method filters too severely the excitation when $a=1$ ($k_c^{\mathrm{FAT}}=k_f$) and underestimates the energy of the acoustic field from 1 kHz, it does not filter enough when $a=2$ ($k_c^{\mathrm{FAT}}=2\,k_f$) and overestimates the force from the same frequency. The latter effect is due to the noise which is mainly located in the high

Table 4
Spatial and temporal parameters for the simulation.

Dimensions	$L_x=L_y=1$ m	Sampling frequency	$f_e=20$ kHz
Discretization	$\Delta_x=\Delta_y=1.5$ cm	Number of samples	$N=5000$

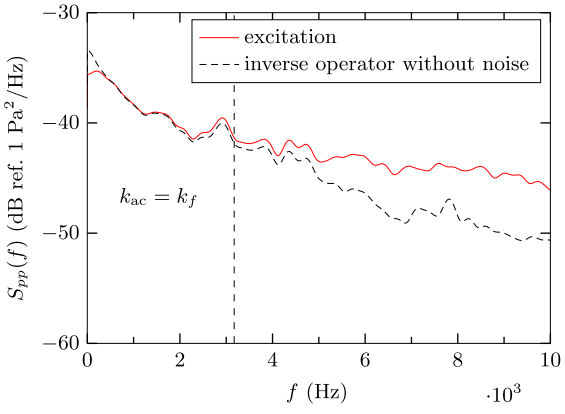

Fig. 7. Power Spectral Densities (PSDs) of the diffuse field that excites the plate and the pressures identified by the inverse operator without noise on the displacement field (reference solution of FAT).

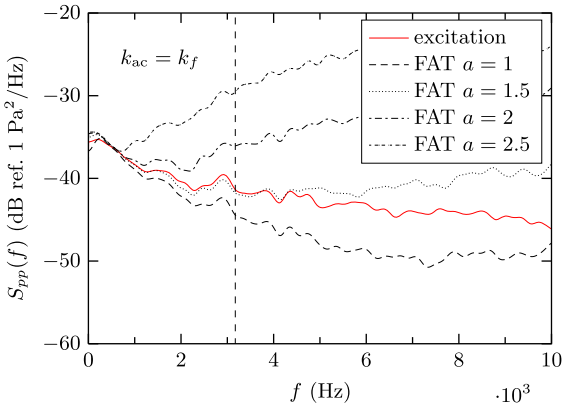

Fig. 8. Influence of the regularization coefficient a in FAT on the identification of the diffuse field that excites a plate (SNR =40 dB).

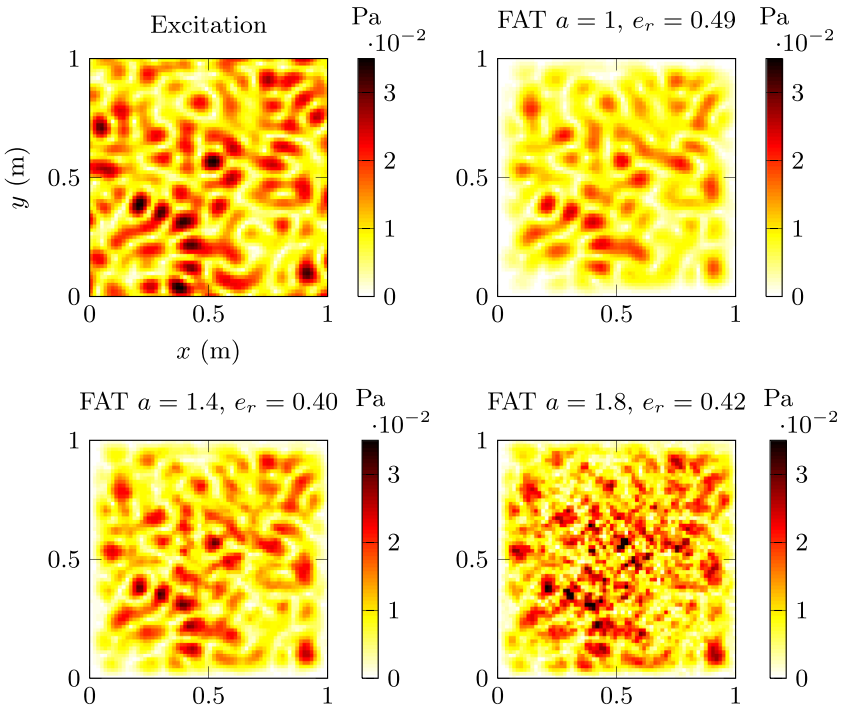

Fig. 9. Influence of the regularization coefficient a on the identified force distributions $|p^{FAT}(x,y,\omega)|$ at the frequency f=2400 Hz (SNR =40 dB). e_r is a spatial error criterion defined in Eq. (26).

wavenumbers (short wavelengths) for which the method is very sensitive. When the coefficient a increases, it takes more into account the high wavenumbers and it amplifies the effect of noise. In addition, this phenomenon is enhanced when the frequency increases because the cutoff of the regularization filter k_c^{FAT} (Eq. (25)) becomes higher.

The spatial representations of the reconstructed fields at a given frequency in Fig. 9 confirm these observations. When a=1, the regularization filter is too strong and the solution is too compact. Conversely, if a=1.8, the solution has a high spatial complexity and does not look like the excitation pressure. In order to evaluate the quality of the identification, a spatial error criterion is introduced

$$e_r(\omega) = \sqrt{\frac{\langle (|p(x,y,\omega)| - |p^{FAT}(x,y,\omega)|)^2 \rangle_s}{\langle |p(x,y,\omega)|^2 \rangle_s}}, \tag{26}$$

where $\langle\,\rangle_s$ is the average in the spatial domain. This criterion is the total error between the excitation and the pressures identified by FAT for a given angular frequency ω. When the regularization is strong (a=1 in Fig. 9) the error is important because the windowing and the filtering produce a significant loss of information. When the regularization is too weak (a=1.8 in Fig. 9) the error is also high because the noise with small wavelengths does not enable to have a good identification. The idea is to find a compromise between these two situations.

With the aim to find an optimal value of a, we chose to study the mean quadratic pressure E_p which is the $L2$ norm of the reconstructed pressures divided by the surface of the domain

$$E_p = \frac{1}{L_x L_y} \int_0^{L_x} \int_0^{L_y} S_{pp}^{\mathrm{FAT}}(x, y, \omega)\, \mathrm{d}x\, \mathrm{d}y, \tag{27}$$

with the Power Spectral Density (PSD) $S_{pp}^{\mathrm{FAT}}(x, y, \omega)$ of the identified pressures:

$$S_{pp}^{\mathrm{FAT}}(x, y, \omega) = \mathrm{E}[|p^{\mathrm{FAT}}(x, y, \omega)|^2]. \tag{28}$$

This indicator is one of the parameters studied in the regularization of inverse or ill-posed problems such as in the L-curve method [26] but these techniques require the calculations of least-square residues which involve to solve the direct problems and to know the boundary conditions and the excitations outside the observed area. Here, the local aspect of the method FAT must be kept and unlike the L-curve method, the energy of the reconstructed pressures is simply analyzed without calculating the direct problem.

The inverse problem is applied several times for a given frequency, by varying the value of coefficient a. The energy of the reconstructed field E_p is calculated for each case. Results are shown in Fig. 10(a) for the frequency $f=2400$ Hz (the same as in Fig. 9) and for three different levels of noise applied to the displacement field. In all three cases, when a is small, the solution has a very low energy, because the filtering is too high. When a increases, the energy stabilizes before rising sharply. For these values, the noise interferes with the identification of the pressure field. Finally, the optimum is in the area where the energy is stabilized, just before the strong change of curvature. One way to find it is to detect the minimum of the derivative of E_p as a function of a (see Fig. 10(b)). For example, the optimum is obtained for $a=1.4$ when the SNR is equal to 40 dB and this solution seems intuitively the best in Fig. 9. Of course the higher the SNR, the greater the optimal value.

The optimum regularization parameter a can be obtained for all frequencies. This requires computing only the inverse problem by varying a and calculating the mean quadratic pressure for each frequency. As shown in Fig. 11, if the SNR is lower, the optimal value is smaller in order to regularize correctly the inverse problem. Similarly, with increasing frequency, the optimized regularization parameter decreases to limit the impact of noise in the high wavenumbers.

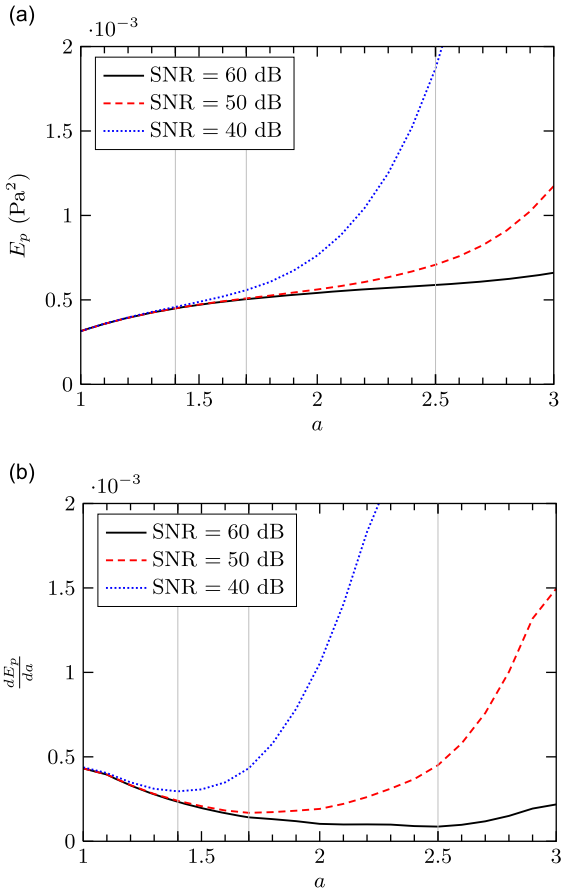

Fig. 10. (a) Mean quadratic pressure and (b) its derivative with respect to a of the force field identified by FAT at the frequency $f=2400$ Hz. Three different noise levels are applied to the displacement field. The vertical lines correspond to the optimal values of a (minima of the derivative).

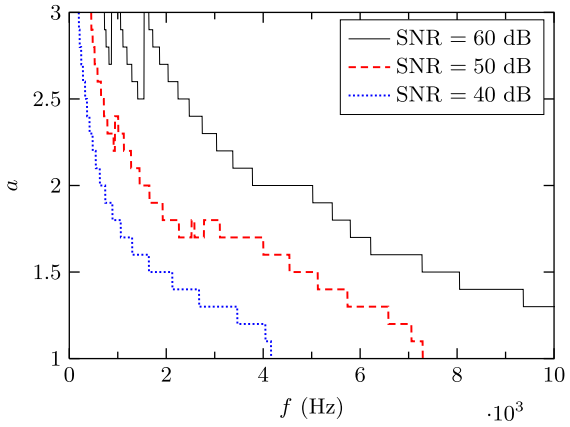

Fig. 11. Optimal value of a as a function of frequency for three different noise levels applied to the displacement field.

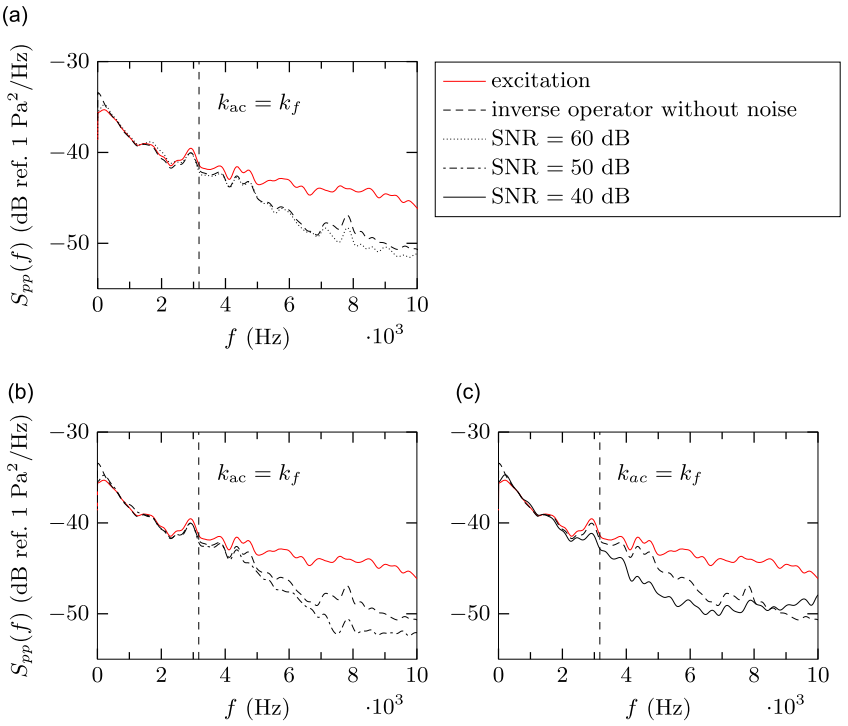

Fig. 12. PSD of the diffuse fields reconstructed by the optimized FAT for a SNR equal to (a) 60 dB, (b) 50 dB and (c) 40 dB. The optimal values of the regularization parameter a are those presented in Fig. 11.

Fig. 12 shows the PSD of the pressures identified with FAT optimized by the calculation of the mean quadratic pressure E_p. The regularization coefficients are those of Fig. 11. The first point is that the solutions obtained through the optimization tend toward the reference (inverse operator without noise). In this way, the method is able to reconstruct the diffuse field up to about 5 kHz with an SNR of 60 or 50 dB, and up to 3.5 kHz for a SNR of 40 dB (to an accuracy of 2 dB). But above all, this optimizing technique with the analysis of the mean quadratic pressure E_p and a regularization coefficient a that depends on frequency ensures a complete identification of the diffuse field up to the acoustic coincidence. For example, a comparison between Fig. 12(c) where this technique is used and Fig. 8 where the choice of the coefficient is arbitrary and independent of the frequency shows that for a given SNR this technique greatly improves FAT.

4.2.2. Identification of the turbulent wall pressures: the Corcos model and the diffuse field

In this section, the identification of turbulent wall pressure is studied. A second simulation is performed with the Corcos model and the diffuse acoustic field of Eq. (10). All simulation parameters are given in Tables 1–3. Results are shown in Fig. 13. They compare the wavenumber–frequency spectra of the excitation signals $p(x,y,t)$ and the pressures $p^{\mathrm{FAT}}(x,y,t)$ identified by FAT when the measured displacement field has a SNR of 40 dB. Thanks to the wavenumber filtering of the

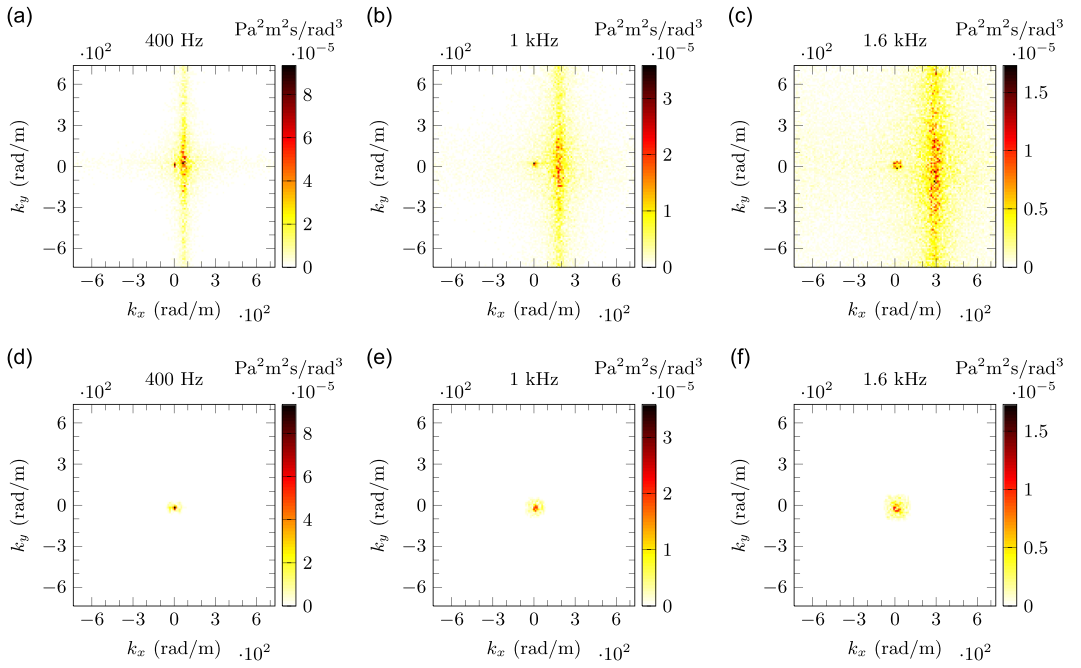

Fig. 13. Wavenumber–frequency spectra $S_{pp'}(k_x, k_y, \omega)$ of the TBL excitation for (a) 400 Hz, (b) 1 kHz, (c) 1.6 kHz and wavenumber–frequency spectra $S_{pp'}^{\mathrm{FAT}}(k_x, k_y, \omega)$ of the pressures identified by FAT (a=1.5, SNR =40 dB) for the same frequencies (d) 400 Hz, (e) 1 kHz and (f) 1.6 kHz.

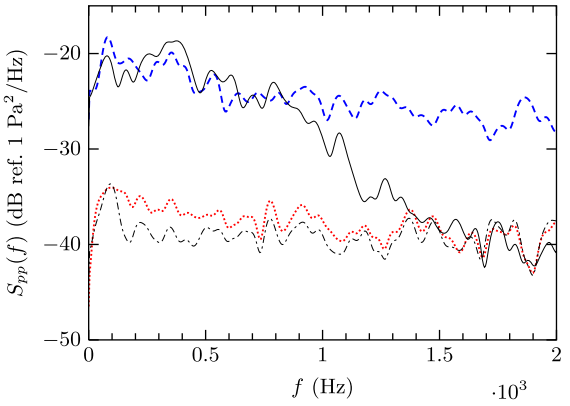

Fig. 14. PSD of the TBL excitation: aerodynamic (- - - dashed line) and acoustic (· · · dotted line) components; the pressures reconstructed by the inverse operator without noise (—— solid line) and by the optimized FAT (- · -) from the noisy displacement (SNR =40 dB).

method, the solution of the inverse problem does not identify the aerodynamic component but highlights very accurately the acoustic part: for the three studied frequencies in Fig. 13, it is possible to reconstruct the acoustic component in terms of amplitude and bandwidth.

To generalize these observations, the PSD calculated at one point is plotted in Fig. 14 where the acoustic and aerodynamic components represent the excitation obtained by the signal synthesis. The solid curve corresponds to the spectrum of the pressures identified by applying the inverse operator in Eq. (24) without noise on the displacement field and then without any regularization step (wavenumber filtering and spatial windowing). This curve confirms the effect of the filtering provided by the discretization of the inverse operator that isolates the acoustic energy from 1.4 kHz. Moreover, this phenomenon is accentuated when the frequency increases as the aerodynamic part moves away in the very high wavenumbers. According to the results presented in Section 4.2.1, the method could isolate and identify the acoustic component up to 5 kHz.

For lower frequencies, it captures the acoustic component and some part of the aerodynamic component because the convection wavenumber k_{conv} is closer to the flexural wavenumber k_f (see Fig. 6). However, applying the optimized FAT presented above to the noisy signals allows us to reconstruct only the acoustic part in these low frequencies because of the additional wavenumber filtering in the regularization step. Indeed, according to Fig. 15, the optimization method imposes

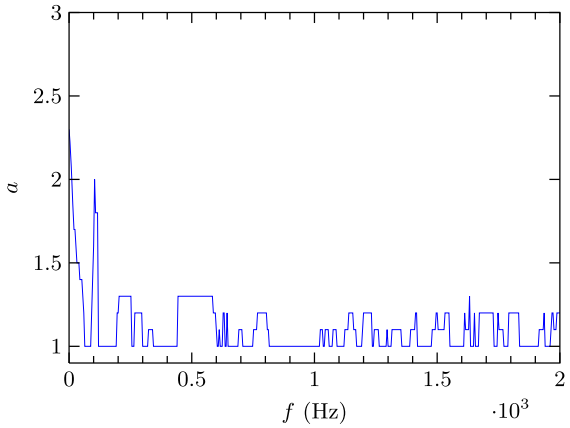

Fig. 15. Optimal value of a as a function of frequency (SNR $=$40 dB). These values are used in the optimized FAT of Fig. 14.

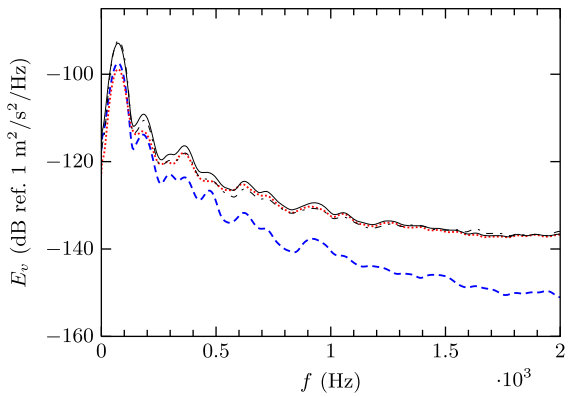

Fig. 16. Mean square velocity of the plate excited (· · ·) by the acoustic component, (- - -) by the aerodynamic part, (——) by both components and (- · -) by the pressure identified by the inverse problem.

a strict regularization in these frequencies in order to eliminate the short wavelengths related to the noise and to the aerodynamic component.

An advantage of this experimental technique is that the plate is very sensitive to the acoustic part. This sensitivity can be highlighted by analyzing the mean square velocity of the structure given by

$$E_v = \frac{1}{L_x L_y} \int_0^{L_x} \int_0^{L_y} S_{vv}(x, y, \omega)\, \mathrm{d}x\, \mathrm{d}y, \tag{29}$$

with $S_{vv}(x, y, \omega)$ being the PSD of the plate velocity. Fig. 16 shows the evolution of E_v as a function of frequency for the plate excited (1) by the acoustic component, (2) by the aerodynamic part, (3) by both components and (4) by the pressure identified by the inverse problem. At low frequencies, up to approximately 200 Hz, the mean square velocity of the plate excited by the aerodynamic component is almost equal to that corresponding to the acoustic part. When the frequency increases, this high-wavenumber component is too far from the flexural wavenumber k_f and the low acoustic part becomes the dominant source. This dominance is so high from about 600 Hz that the mean square velocity of the plate excited by both components is almost equal to that excited only by the acoustic part. This high sensitivity of the panel to the acoustic component over this wide frequency band makes the plate be a sensor with a better SNR to measure low wavenumbers in the excitation.

Finally, the curve of Fig. 16 representing the mean square velocity of the plate excited by the pressure calculated by FAT shows that the method identifies the main sources of vibration: the aerodynamic and acoustic components in low frequency and only the acoustic part in higher frequency.

5. Conclusion

This paper presents a numerical experiment for identifying the wall pressures generated by TBL. The excitation, resulting from the synthesis of signals by the Cholesky decomposition, is a simplified model combining the Corcos model and an

acoustic diffuse field. In this particular case, the results clearly show that FAT allows one to reconstruct exclusively the low wavenumbers and thus the acoustic component of the excitation. A new method for optimizing the regularization of FAT, based on the analysis of the mean quadratic pressure of the reconstructed fields, is introduced and improves this inverse method. Thus, the optimized solution obtained provides an identification of the acoustic component up to the acoustic coincidence. In addition, this optimization does not require to calculate a theoretical direct problem as it is usually in the L-curve method and the local character of FAT is preserved (there is no need to know the boundary conditions and the dynamic behaviour of all the structure). An important perspective is to generalize these observations to other kinds of turbulent flows or structures such as shells [27,28]. It is also planned to test the method on a real experience where the displacement field is measured on the other side of the wall by a non-intrusive technique as real-time near-field acoustic holography [29,30]. Indeed, the coupling of FAT with the standard near-field acoustic holography had already been tested [31] and appeared to give good results.

References

[1] C. Maury, P. Gardonio, S.J. Elliott, A wavenumber approach to modelling the response of a randomly excited panel. Part I. General theory, *Journal of Sound and Vibration* 252 (2002) 83–113.
[2] W. Graham, Boundary layer induced noise in aircraft. Part I. The flat plate model, *Journal of Sound and Vibration* 192 (1996) 101–120.
[3] X. Gloerfelt, J. Berland, Direct computation of turbulent boundary layer noise, *15th AIAA/CEAS AeroAcoustics Conference*, Miami, FL, 11–13 May 2009, AIAA Paper 2009-3401.
[4] G.M. Corcos, Resolution of pressure in turbulence, *The Journal of the Acoustical Society of America* 35 (1963) 192–199.
[5] D.M. Chase, Modeling the wavevector–frequency spectrum of turbulent boundary layer wall pressure, *Journal of Sound and Vibration* 70 (1980) 29–67.
[6] D.M. Chase, The character of the turbulent wall pressure spectrum at subconvective wavenumbers and a suggested comprehensive model, *Journal of Sound and Vibration* 112 (1987) 125–147.
[7] B. Arguillat, D. Ricot, C. Bailly, G. Robert, Measured wavenumber: *frequency spectrum associated with acoustic and aerodynamic wall pressure fluctuations*, *The Journal of the Acoustical Society of America* 128 (2010) 1647–1655.
[8] C. Pezerat, J. Guyader, Two inverse methods for localization of external sources exciting a beam, *Acta Acustica* 3 (1995) 1–10.
[9] F.A. Aupperle, R.F. Lambert, On the utilization of a flexible beam as a spatial filter, *Journal of Sound and Vibration* 24 (1972) 259–267.
[10] N.C. Martin, P. Leehey, Low wavenumber wall pressure measurements using a rectangular membrane as a spatial filter, *Journal of Sound and Vibration* 52 (1977) 95–120.
[11] F. Chevillotte, Q. Leclère, N. Totaro, C. Pézerat, P. Souchotte, G. Robert, Identification d'un champ de pression pariétale induit par un écoulement turbulent à partir de mesures vibratoires, *Congrès Français d'Acoustique*, 2010.
[12] W.K. Blake, *Mechanics of Flow-Induced Sound and Vibration*, vols. 1 and 2, Academic Press, New York, 1986.
[13] B. Arguillat, Étude Expérimentale et Numérique de Champs de Pression Pariétale dans l'Espace des Nombres d'onde, Avec Application aux Vitrages Automobiles, PhD Thesis, Ecole Centrale de Lyon, Laboratoire de Mécanique des Fluides et d'Acoustique, 2006.
[14] J.-L. Guyader, *Vibration in Continuous Media*, ISTE, United Kingdom, 2006.
[15] Y.F. Hwang, W. Bonness, S. Hambric, Comparison of semi-empirical models for turbulent boundary layer wall pressure spectra, *Journal of Sound and Vibration* 319 (2009) 199–217.
[16] M. Goody, Empirical spectral model of surface pressure fluctuations, *AIAA Journal* 42 (2004) 1788–1794.
[17] T. Farabee, M. Casarella, Spectral features of wall pressure fluctuations beneath turbulent boundary layers, *Physics of Fluids A: Fluid Dynamics* 3 (1991) 2410.
[18] M. Howe, Surface pressures and sound produced by turbulent flow over smooth and rough walls, *The Journal of the Acoustical Society of America* 90 (1991) 1041–1047.
[19] H. Nélisse, J. Nicolas, Characterization of a diffuse field in a reverberant room, *The Journal of the Acoustical Society of America* 101 (1997) 3517–3524.
[20] L.E. Wittig, A. Sinha, Simulation of multicorrelated random processes using the FFT algorithm, *The Journal of the Acoustical Society of America* 58 (1975) 630.
[21] D. Ricot, A. Hekmati, P. Druault, Analysis of the Vibroacoustic Behavior of a Plate Excited by Synthesized Aeroacoustic Pressure Fields, Acoustics, 2012.
[22] N. Totaro, Caractérisation de Sources Aérodynamiques et Sous-Structuration Pour la Méthode SEA, PhD Thesis, 2004.
[23] C. Pézerat, J.-L. Guyader, Force analysis technique: *reconstruction of force distribution on plates*, *Acta Acustica United with Acustica* 86 (2000) 322–332.
[24] Q. Leclère, C. Pézerat, Vibration source identification using corrected finite difference schemes, *Journal of Sound and Vibration* 331 (2012) 1366–1377.
[25] C. Pézerat, T. Loyau, J.-L. Guyader, Characterisation of vibration sources on a set of plates using the RIFF techniques, *Noise Control Engineering Journal* 50 (2002) 50.
[26] P. Hansen, Analysis of discrete ill-posed problems by means of the L-curve, *SIAM Review* (1992) 561–580.
[27] M.C. Djamaa, N. Ouelaa, C. Pézerat, J.-L. Guyader, Mechanical radial force identification of a finite cylindrical shell by an inverse method, *Acta Acustica United with Acustica* 92 (2006) 398–405.
[28] M.C. Djamaa, N. Ouelaa, C. Pézerat, J. Guyader, Reconstruction of a distributed force applied on a thin cylindrical shell by an inverse method and spatial filtering, *Journal of Sound and Vibration* 301 (2007) 560–575.
[29] J.-H. Thomas, V. Grulier, S. Paillasseur, J.-C. Pascal, Real-time near-field acoustic holography for continuously visualizing nonstationary acoustic fields, *The Journal of the Acoustical Society of America* 128 (2010) 3554–3567.
[30] S. Paillasseur, J.-H. Thomas, J. Pascal, Regularization for improving the deconvolution in real-time near-field acoustic holography, *The Journal of the Acoustical Society of America* 129 (2011) 3777–3787.
[31] C. Pézerat, Q. Leclère, N. Totaro, M. Pachebat, Identification of vibration excitations from acoustic measurements using near field acoustic holography and the force analysis technique, *Journal of Sound and Vibration* 326 (2009) 540–556.